we use the orientation averaged

$$\rho_{\mathrm{iso}}(z) = \frac{1}{3}\rho_{\perp}(z) + \frac{2}{3}\rho_{\parallel}(z) \tag{2}$$

where $\rho_{\perp}(z)$ and $\rho_{\perp}(z)$ are the relative local density of states for dipoles oriented perpendicular and parallel to the mirror surface, respectively.[40]

The fitted $\gamma_{\mathrm{tot}}^{\mathrm{iso}}(z)$ (calculated for dipoles embedded 10 nm below the PMMA/air interface to account for the bead material) is plotted as the red line in Fig. 6, left. We find fair agreement with the experimental data. For distances exceeding the vacuum emission wavelength of the emitter (due to the wedge index this encompasses several oscillations in the LDOS) the oscillation amplitude of the local density of states decreases and becomes comparable to the uncertainty in fitted total decay rates. We hence use the emitter's emission wavelength as upper bound on distances plotted. By plotting decay rate versus LDOS, instead of decay rate versus *z*, we can directly find the radiative and nonradiative decay rate from the slope and ordinate intersection of the linear dependence, respectively (Fig. 7). Throughout this work, error bars on rates and efficiencies result from the LDOS fit, taking into account error bars on the decay rate fitted at each vertical distance. For the fluorescent beads, we find an intrinsic radiative decay rate of $(0.10 \pm 0.01)\,\mathrm{ns}^{-1}$ and a nonradiative decay rate of $(0.07 \pm 0.01)\,\mathrm{ns}^{-1}$. The hypothetical radiative decay rate for this emitter in vacuum, extrapolates to a radiative rate of $(0.15 \pm 0.01)\,\mathrm{ns}^{-1}$ in its PMMA host. We extract a quantum efficiency

$$q.e. \equiv \gamma_{\mathrm{rad}}/(\gamma_{\mathrm{rad}} + \gamma_{\mathrm{nonrad}}) \tag{3}$$

of $61\% \pm 7\%$ for the emitter hypothetically in vacuum, and around $70\% \pm 6\%$ for the emitter embedded in its bulk host material, i.e., bulk PMMA.

In many applications targeting the use of metamaterials and plasmonics to control emitters, one preferentially does not use emitters with emission wavelengths at 605 nm, such as the beads, but rather emitters emitting further into the near-infrared. Recent reports by Curto et al.[29] propose that CdSeTe/ZnS quantum dots emitting at around 800 nm are ideally suited single emitters for

plasmonic applications, as they are ultrabright. The fluorescence time delay histogram retrieved from a FLIM image of an ensemble of Invitrogen Qdot 800 ITK carboxyl quantum dots does not resemble a single exponential decay. Here, we make use of the fact that an ensemble of quantum dots should be modeled with a continuous distribution of decay rates.[41,42] More precisely, the natural logarithm of decay rates γ is assumed to be normally distributed according to the log-normal distribution

$$p(\gamma) = A \cdot \exp\left(\frac{\ln^2(\gamma/\gamma^{\mathrm{mf}})}{w^2}\right). \tag{4}$$

The normalization constant A is given by the condition $\int_0^\infty p(\gamma)d\gamma = 1$. The dimensionless width w can be rewritten as the width of the rate distribution for which $p = 1/e$:

$$\Delta\gamma = 2\gamma^{\mathrm{mf}} \sinh w. \tag{5}$$

Hence, the two free parameters of our fit-model are the most frequent decay rate γ^{mf}, at which the log-normal distribution is centered, and the rate distribution width $\Delta\gamma$. The fitted most frequent decay rates are shown in Fig. 6, center and Fig. 7, center together with a fit to the LDOS for isotropically oriented dipoles. We would like to point out that as we fit the Drexhage model to just the retrieved γ^{mf}, the extracted values we quote quantify only the most frequently occurring decay rates and quantum efficiencies, and not the width of the underlying distribution. For the quantum dots we find a most frequent intrinsic radiative decay rate of $(5.46 \pm 0.51)\,\mu\mathrm{s}^{-1}$, a most frequent nonradiative decay rate of $(0.62 \pm 0.66)\,\mu\mathrm{s}^{-1}$ and a most frequent quantum efficiency of $90\% \pm 11\%$ for the emitter hypothetically in vacuum. In its actual bulk host material, i.e., bulk S1813 we find a most frequent radiative decay rate of $(9.00 \pm 0.84)\,\mu\mathrm{s}^{-1}$ and a quantum efficiency of around $94\% \pm 7\%$.

The high quantum efficiency for these quantum dots makes them exceptionally promising for plasmon quantum optics, since operating at 800 nm optimizes the emission frequency to be at the intersection of low plasmon loss, yet efficient silicon detection. The high quantum efficiency is surprising given that the solvent/ligand exchange to aqueous condition, and operation of quantum

dots unprotected against oxygen as in our experiment usually adversely affects the photophysical properties. Here we note that measuring quantum efficiency via modulation of radiative lifetime selectively measures the quantum efficiency of the ensemble of dots that radiate, i.e., that are not temporarily or permanently dark due to (photo)chemical processes such as bleaching or blinking. This property should be contrasted to absorption/emission brightness measurements that report quantum efficiency as the fraction of absorbed photons that is converted into radiated photons by an ensemble of nanocrystals. In such measurements a mixture of a dark subensemble that absorbs but does not emit with a subensemble of unit-efficiency emitters is indistinguishable from a homogeneous sample of emitters with below-unit quantum efficiency. The conclusion from our measurement is that those dots that are not (photo)chemically altered by an oxygen-rich or aqueous environment, retain high quantum efficiency. A similar conclusion that the quantum efficiency of those dots that radiate is much higher than the ensemble efficiency obtained from a absorption/emission brightness measurements was also reached by Leistikow,[23] for CdSe quantum dots emitting around 600 nm, with efficiencies between 66% and 89%. Evidently, the CdSeTe/ZnS core shell dots emitting at 800 nm have a 6-fold longer lifetime compared to CdSe quantum dots, consistent with observations by Vion et al.[35] It is remarkable that the (bright) 800 nm dots in our work manage to retain a very high quantum efficiency, despite this 6-fold longer lifetime.[23]

An interesting alternative to the quantum dots, which while efficient, have a slow and non-single exponential decay, could be DBT with an emission wavelength of $\approx 750\,\mathrm{nm}$.[36,37] DBT was recently reported to be ultrastable and ultrabright as an emitter at room temperature.[37] In contrast to Toninelli's observations on single molecules, we observe a non-single exponential decay trace for ensembles of DBT molecules. Therefore, we apply the same analysis scheme as for the quantum dots: log-normally distributed decay rates.[41] In this manner we find a most frequent intrinsic radiative decay rate of $(0.05 \pm 0.01)\,\mathrm{ns}^{-1}$, a most frequent nonradiative decay rate of $(0.27 \pm 0.01)\,\mathrm{ns}^{-1}$ and a most frequent quantum efficiency of $16\% \pm 3\%$, when calculating with the radiative rate extrapolated to vacuum. Decay rate data and LDOS fit for DBT are shown in Fig. 6, right and Fig. 7, right. Since DBT is always used in anthracene, it is useful to extract the

quantum efficiency in bulk anthracene. Correcting for the index of refraction of anthracene, we find a most frequent radiative decay rate of $(0.09 \pm 0.02)\,\mathrm{ns}^{-1}$ and a quantum efficiency around $24\% \pm 4\%$.

The moderate to low quantum efficiency that our measurement retrieves for DBT is surprising, since Toninelli et al.[37] have reported very high count rates from single DBT molecules in anthracene at room temperature. In saturation, they reported detecting photons at a rate of up to 0.5% of the inverse lifetime. A quantum efficiency of around 25% is within, but at the low end of, the range of values that are consistent with the observation of Toninelli et al.,[37] depending on the actual microscope collection efficiency (state of the art: a few percent at 800 nm). We note that the observations of Toninelli et al.[37] are strictly for individual molecules selected to be ideal in the sense of being long lived, which likely selects molecules from those 10% best incorporated in the anthracene matrix. While agreement with LDOS theory for isotropic dipole orientations is good, we found poor agreement of decay rate data to LDOS lineshapes for specific dipole orientations, despite reports of preferential orientation for this system.[37] This further highlights that we probe a heterogeneously distributed ensemble of emitters, as opposed to selecting particular emitters as in single molecule experiments.[37] From observation of the film quality, we note that it was difficult to obtain homogeneous anthracene crystal films throughout the entire wedge length, both on the wedge material as well as on clean cover slips.

Tab. 1 summarizes the retrieved radiative and nonradiative decay constants and respective quantum efficiencies for all three fluorophores.

Table 1: Table of emitter properties retrieved from our Drexhage experiments. As we assumed a log-normal distribution of decay rates for the probed Invitrogen Qdot and DBT ensembles, the stated decay rates and quantum efficiencies are the ones which are most-frequent (superscript 'mf'). Radiative decay rates and quantum efficiencies are quoted for the emitters embedded in their respective host medium: PMMA (Fluospheres), S1813 (quantum dots), and anthracene (DBT).

	Invitrogen Fluospheres F8801	Invitrogen Qdot 800 ITK carboxyl	DBT in AC
$\gamma_{\mathrm{rad,host}}^{\mathrm{mf}}$	$(0.15 \pm 0.01)\,\mathrm{ns}^{-1}$	$(9.00 \pm 0.84)\,\mu\mathrm{s}^{-1}$	$(0.09 \pm 0.02)\,\mathrm{ns}^{-1}$
$\gamma_{\mathrm{nonrad}}^{\mathrm{mf}}$	$(0.07 \pm 0.01)\,\mathrm{ns}^{-1}$	$(0.62 \pm 0.66)\,\mu\mathrm{s}^{-1}$	$(0.27 \pm 0.01)\,\mathrm{ns}^{-1}$
$q.e._{\mathrm{host}}^{\mathrm{mf}}$	$71\% \pm 6\%$	$94\% \pm 7\%$	$24\% \pm 4\%$

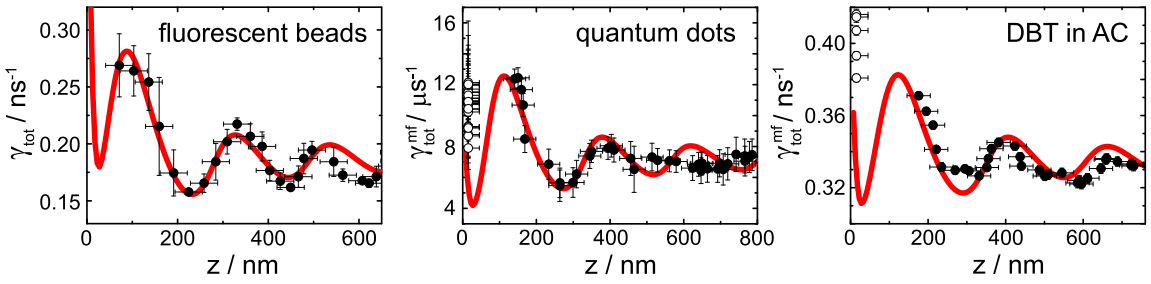

Figure 6: Fitted total decay rates γ_{tot}^{mf} vs distance to the mirror z (black dots). White circles are fitted values to decay traces gathered right on top of the mirror (next to the wedge, $z \approx 0$) and plotted at a fixed height offset from zero for good visibility. The red lines indicate fitted relative LDOS ρ_{iso} for isotropically oriented dipoles.

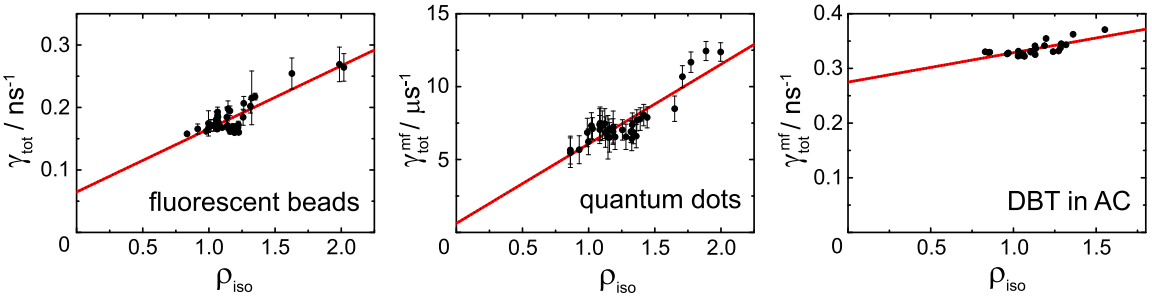

Figure 7: Total decay rates γ_{tot}^{mf} vs relative LDOS ρ_{iso} for isotropically oriented dipoles. The red lines indicate fits according to eq.1.

Conclusions and outlook

In conclusion, we have demonstrated that gray-tone UV-lithography[26] provides a facile method to create samples to calibrate ensembles of emitters. The essential steps of this method are (1) gray-tone lithography to create S1813 or PMMA polymer wedges on flat reflective substrates, such as an Ag or Au mirror, (2) a homogeneous dispersal method to distribute fluorophores on the wedge, and (3) lifetime measurements along the length of the wedge to effectuate Drexhage experiments.[19] Previous methods rather used controlled stepped etching into substrates that had the light sources embedded in them, i.e., a material-specific technique suited for III-V sources,[24] or depended on the creation of a large but discrete set of substrates with different deposition thicknesses of dielectric spacer layer.[23] Instead, our method allows to create a continuous wedge on a single substrate. Our method can thus be of large use for calibrating a range of fluorophores for applications ranging from quantum optics, to organic and inorganic light emitting diodes. We note that a large range of variations is easily implemented. For instance, if surface chemistry means it is advantageous to first deposit the fluorophores on glass, then create a wedge, and then deposit a mirror, this is equally easily implemented. Beyond calibration of unknown emitters using a known LDOS, the same method is also of large interest to do the reverse, i.e., to measure an *unknown* LDOS using a calibrated emitter. Indeed, in plasmonics, metamaterials, and the new field of metasurfaces, one frequently encounters questions that revolve around the LDOS at controlled distance. Consider for instance the optimization of light emitting diodes by plasmon particle array surfaces[6,8,9] or extraordinary transmission gratings.[43] The question at which distance one should optimally place the emitters to both enhance outcoupling, radiative rate, and quantum efficiency is of key importance, yet difficult to address experimentally. Likewise, the fundamental study of effective medium parameters of metamaterials come to mind. Photonic metamaterials are artificial materials with periodic arrangements of subwavelength scatterers aimed at arbitrary control of permittivity ε and permeability μ to realize perfect lenses and invisibility cloaks via transformation optics.[44–47] For a wide range of metamaterials ε and μ have been reported,[48–50] showing that it is indeed possible to obtain, e.g., effectively negative μ. Effective medium constants are commonly

retrieved from *far field* experiments. Since metamaterials have intrinsic near field benefits, it is interesting to test whether these effective material parameters retrieved from far field measures such as transmittance and reflectance, are still valid in the near field. Using our wedge technique one can continuously sweep source height through the near field zone to examine the transition from resolving individual building blocks to resolving just the effective parameters.[51,52] The polymer wedges that we fabricate can indeed also be readily made on patterned surfaces, thereby opening the road to controllably vary the near-field spacing and measure the metamaterial LDOS. This method is complementary to elaborate near-field scanning methods.[34] The loss of lateral resolution in our method compared to near-field scanning is offset by the ease of use of the gray-tone lithography wedge technique, and the fact that in many applications (e.g., plasmon enhanced LEDs) the only useful quantity would anyway be of ensemble averaged nature.

Acknowledgement

We thank Martin Frimmer for initial help with lifetime measurements, Gijs Vollenbroek for assistance with sample fabrication, and Dr. Toninelli for kindly sharing her experience with depositing DBT in anthracene. This work is part of the research programme of the Foundation for Fundamental Research on Matter (FOM), which is part of the Netherlands Organisation for Scientific Research (NWO). AFK acknowledges a NWO-Vidi fellowship.

References

(1) Friend, R. H.; Gymer, R. W.; Holmes, A. B.; Burroughes, J. H.; Marks, R. N.; Taliani, C.; Bradley, D. D. C.; Santos, D. A. D.; Bredas, J. L.; Logdlund, M.; Salaneck, W. R. *Nature* **1999**, *397*, 121–128.

(2) Alivisatos, A. P. *Science* **1996**, *271*, 933–937.

(3) Nakamura, S. *Sol. Stat. Comm.* **1997**, *102*, 237–248.

(4) Murray, C. B.; Norris, D. J.; Bawendi, M. G. *J. Am. Chem. Soc.* **1993**, *115*, 8706–8715.

(5) Soukoulis, C. M., Ed. *Photonic Crystals and Light Localization in the 21st Century*; Kluwer Academic Publishers, 2001.

(6) Zayats, A. V.; Smolyaninov, I. I.; Maradudin, A. A. *Phys. Rep.* **2005**, *408*, 131–314.

(7) Mühlschlegel, P.; Eisler, H.-J.; Martin, O. J. F.; Hecht, B.; Pohl, D. W. *Science* **2005**, *308*, 1607–1609.

(8) Muskens, O. L.; Giannini, V.; Sánchez-Gil, J. A.; Gómez Rivas, J. *Nano Lett.* **2007**, *7*, 2871–2875.

(9) Vecchi, G.; Giannini, V.; Gómez Rivas, J. *Phys. Rev. Lett.* **2009**, *102*, 146807.

(10) Lodahl, P.; van Driel, A. F.; Nikolaev, I. S.; Irman, A.; Overgaag, K.; Vanmaekelbergh, D.; Vos, W. L. *Nature* **2004**, *430*, 654–657.

(11) Sprik, R.; van Tiggelen, B. A.; Lagendijk, A. *Eur. Phys. Lett.* **1996**, *35*, 265–270.

(12) Novotny, L.; Hecht, B. *Principles of Nano-Optics*; Cambridge University Press, Cambridge, 2006.

(13) Bertet, P.; Auffeves, A.; Maioli, P.; Osnaghi, S.; Meunier, T.; Brune, M.; Raimond, J. M.; Haroche, S. *Phys. Rev. Lett.* **2002**, *89*, 200402.

(14) Lounis, B.; Orrit, M. *Rep. Prog. Phys.* **2005**, *68*, 1129–1179.

(15) Lakowicz, J. R. *Principles of Fluorescence Spectroscopy*; Springer, 2006.

(16) Drexhage, K. H.; Kuhn, H.; Schäfer, F. P. *Ber. Buns. f. Phys. Chem.* **1968**, *72*, 329.

(17) Drexhage, K. *J. Lumin.* **1970**, *1 & 2*, 693–701.

(18) Amos, R. M.; Barnes, W. L. *Phys. Rev. B* **1997**, *55*, 7249–7254.

(19) Snoeks, E.; Lagendijk, A.; Polman, A. *Phys. Rev. Lett.* **1995**, *74*, 2459–2462.

(20) Buchler, B. C.; Kalkbrenner, T.; Hettich, C.; Sandoghdar, V. *Phys. Rev. Lett.* **2005**, *95*, 063003.

(21) Chance, R. R.; Prock, A.; Silbey, R. *Adv. Chem. Phys.* **1978**, *37*, 1–65.

(22) de Dood, M. J. A.; Slooff, L. H.; Polman, A.; Moroz, A.; van Blaaderen, A. *Appl. Phys. Lett.* **2001**, *79*, 3585–3587.

(23) Leistikow, M. D.; Johansen, J.; Kettelarij, A. J.; Lodahl, P.; Vos, W. L. *Phys. Rev. B* **2009**, *79*, 045301.

(24) Stobbe, S.; Johansen, J.; Kristensen, P. T.; Hvam, J. M.; Lodahl, P. *Phys. Rev. B* **2009**, *80*, 155307.

(25) Wang, Q.; Stobbe, S.; Lodahl, P. *Phys. Rev. Lett.* **2011**, *107*, 167404.

(26) Christophersen, M.; Phlips, B. F. *Appl. Phys. Lett.* **2008**, *92*, 194102.

(27) Akimov, A. V.; Mukherjee, A.; Yu, C. L.; Chang, D. E.; Zibrov, A. S.; Hemmer, P. R.; Park, H.; Lukin, M. D. *Nature* **2007**, *450*, 402–406.

(28) Chang, D. E.; Sørensen, A. S.; Demler, E. A.; Lukin, M. D. *Nat. Phys.* **2007**, *3*, 807–812.

(29) Curto, A. G.; Volpe, G.; Taminiau, T. H.; Kreuzer, M. P.; Quidant, R.; van Hulst, N. F. *Science* **2010**, *329*, 930–933.

(30) Koenderink, A. F. *Nano Lett.* **2009**, *9*, 4228–4233.

(31) Pendry, J. B.; Smith, D. R. *Physics Today* **2004**, *57*, 37–43.

(32) Shalaev, V. M. *Nat. Photon.* **2007**, *1*, 41–48.

(33) Soukoulis, C. M.; Wegener, M. *Nat. Photon.* **2011**, *5*, 523–530.

(34) Frimmer, M.; Chen, Y.; Koenderink, A. F. *Phys. Rev. Lett.* **2011**, *107*, 123602.

(35) Vion, C.; Barthou, C.; Bénalloul, P.; Schwob, C.; Coolen, L.; Gruzintev, A.; Emel'chenko, G.; Masalov, V.; Frigerio, J.-M.; Maître, A. *J. Appl. Phys.* **2009**, *105*, 113120.

(36) Jelezko, F.; Tamarat, P.; Lounis, B.; Orrit, M. *J. Phys. Chem.* **1996**, *100*, 13892–13894.

(37) Toninelli, C.; Early, K.; Bremi, J.; Renn, A.; Götzinger, S.; Sandoghdar, V. *Opt. Express* **2010**, *18*, 6577–6582.

(38) Bajzer, Ž.; Therneau, T. M.; Sharp, J. C.; Prendergast, F. G. *Eur. Biophys. J.* **1991**, *20*, 247–262.

(39) Paulus, M.; Gay-Balmaz, P.; Martin, O. J. F. *Phys. Rev. E* **2000**, *62*, 5797–5807.

(40) Vos, W. L.; Koenderink, A. F.; Nikolaev, I. S. *Phys. Rev. A* **2009**, *80*, 053802.

(41) van Driel, A. F.; Nikolaev, I. S.; Vergeer, P.; Lodahl, P.; Vanmaekelbergh, D.; Vos, W. L. *Phys. Rev. B* **2007**, *75*, 035329.

(42) Nikolaev, I. S.; Lodahl, P.; van Driel, A. F.; Koenderink, A. F.; Vos, W. L. *Phys. Rev. B* **2007**, *75*, 115302.

(43) Ebbesen, T. W.; Lezec, H. J.; Ghaemi, H. F.; Thio, T.; Wolff, P. A. *Nature* **1998**, *391*, 667–669.

(44) Pendry, J. B. *Phys. Rev. Lett.* **2000**, *85*, 3966–3969.

(45) Valentine, J.; Li, J.; Zentgraf, T.; Bartal, G.; Zhang, X. *Nat. Mater.* **2009**, *8*, 568–571.

(46) Ergin, T.; Stenger, N.; Brenner, P.; Pendry, J. B.; Wegener, M. *Science* **2010**, *328*, 337–339.

(47) Zentgraf, T.; Valentine, J.; Tapia, N.; Li, J.; Zhang, X. *Adv. Mater.* **2010**, *22*, 2561–2564.

(48) Shelby, R. A.; Smith, D. R.; Schultz, S. *Science* **2001**, *292*, 77–79.

(49) Dolling, G.; Enkrich, C.; Wegener, M.; Soukoulis, C. M.; Linden, S. *Science* **2006**, *312*, 892–894.

(50) Valentine, J.; Zhang, S.; Zentgraf, T.; Ulin-Avila, E.; Genov, D. A.; Bartal, G.; Zhang, X. *Nature* **2008**, *455*, 376–379.

(51) Kästel, J.; Fleischhauer, M. *Phys. Rev. A* **2005**, *71*, 011804.

(52) Dung, H. T.; Buhmann, S. Y.; Knöll, L.; Welsch, D.-G.; Scheel, S.; Kästel, J. *Phys. Rev. A* **2003**, *68*, 043816.

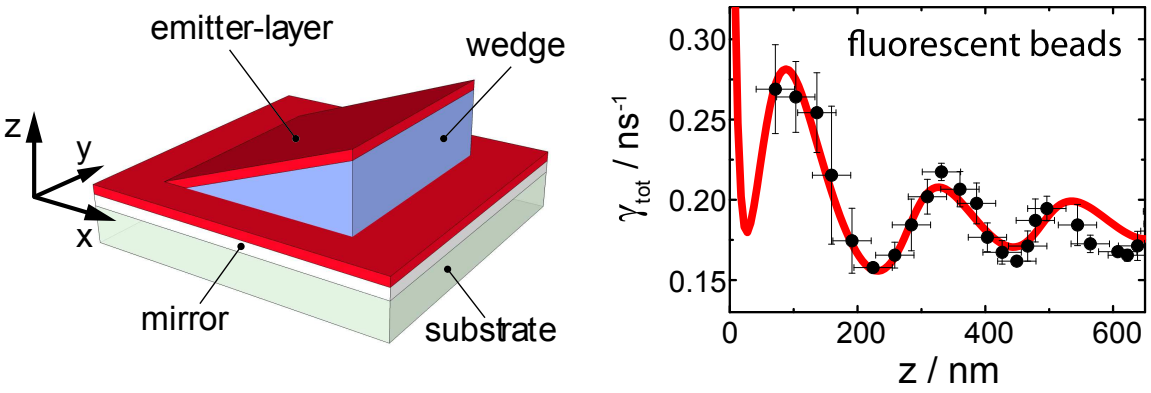

Figure 8: Table of content figure